ISSN: 2281-1346

UNIVERSITÀ DI PAVIA
Department of Economics and Management

DEM Working Paper Series

Modeling Turning Points In Global Equity Market

Daniel Felix Ahelegbey
(Università di Pavia)

Monica Billio
(University of Venice)

Roberto Casarin
(University of Venice)

 # 195 (11-20)

Via San Felice, 5
I-27100 Pavia

economiaweb.unipv.it

Modeling Turning Points In Global Equity Market

Daniel Felix Ahelegbey[a,*], Monica Billio[b], Roberto Casarin[b]

[a] *Department of Economics and Management, University of Pavia, Italy*
[b] *Department of Economics, University of Venice, Italy*

Abstract

Turning points in financial markets are often characterized by changes in the direction and/or magnitude of market movements with short-to-long term impacts on investors' decisions. This paper develops a Bayesian technique to turning point detection in financial equity markets. We derive the interconnectedness among stock market returns from a piece-wise network vector autoregressive model. The empirical application examines turning points in global equity market over the past two decades. We also compare the Covid-19 induced interconnectedness with that of the global financial crisis in 2008 to identify similarities and the most central market for spillover propagation.

Keywords: Bayesian inference, Dynamic Programming, Turning points, Networks, VAR

JEL: C11, C15, C51, C52, C55, C58, G01

1. Introduction

The turn of events in major financial markets since late-February 2020, following the spread of the novel coronavirus (COVID-19) from Wuhan, in China to a global pandemic, is certainly a reminder of how increased interconnectedness between markets over time play a substantial role in the contagion spreading, especially during turbulent times. As a consequence, the degree of comovements in asset markets within and across countries increases in presence of shocks, and shocks propagate to markets across countries and regions, with corresponding impacts on asset prices/returns. A clear understanding of the nature of the linkages and interconnectedness among markets is critical to understand potential contagion. Modeling financial interconnectedness have received much attention, especially after the the global financial crisis of 2007–2009, and the European sovereign debt crisis of 2010–2013 (see Ahelegbey et al., 2016b; Battiston et al., 2012; Billio et al., 2019, 2012; DasGupta and Kaligounder, 2014; Diebold and Yilmaz, 2014; Hautsch et al., 2015).

In investigating the dynamic nature of interconnectedness among institutions and markets, it has become necessary to build models that are flexible to allow also structural changes. For instance, financial institutions are often interconnected through diverse channels, ranging from inter-bank market transfers, direct deposits, relationship lending/borrowing, and exposures to common risk or market factors. These connections can change with time. Turning points in financial markets are often characterized by changes in direction and/or magnitude of market movements with short-to-long term impacts on investors' decisions. These turning points may

*Corresponding author
Email addresses: danielfelix.ahelegbey@unipv.it (Daniel Felix Ahelegbey), billio@unive.it (Monica Billio), r.casarin@unive.it (Roberto Casarin)

occur as a result of changes in policy regimes, fluctuations in underlying market conditions or changes in the financial health of counterparties, leading to widespread implications on the economy and in financial markets. From a modeling perspective, changes in structural relationships affect predictions, as the use of old data becomes counter-productive. However, if the conditions associated with changes in financial markets are similar to past occurrences, then such information can prove helpful by signalling the direction of market conditions. This study contributes to a stream of research useful to identify turning points in multivariate time series to better understand non-stationarity in time series observations (see Bai, 2000; Chib, 1998; Cho and Fryzlewicz, 2015; Pesaran et al., 2006; Qu and Perron, 2007; Ruggieri, 2013).

This paper contributes to the above discussion by advancing a Bayesian technique to turning point detection in financial equity markets. We formalize the derivation of the interconnectedness among stock market returns from a piece-wise vector autoregressive with residual structural equations model (VAR-RSEM). That is, we model the dynamics of the returns by a reduced-form VAR with the residuals as a system of structural equations. Financial time series data usually exhibit contemporaneous dependencies as well as temporal lag relationships over time. The VAR-RSEM specification is designed to account for the contemporaneous, serial, and cross-lagged dependencies beyond what simple stylized facts from historical data can provide. Closely related models have in recent times been applied to infer financial contagion networks (see Ahelegbey et al., 2016a,b; Barigozzi and Brownlees, 2019; Basu and Michailidis, 2015; Bianchi et al., 2019; Billio et al., 2019, 2012; Diebold and Yilmaz, 2014). In a typical moderate to large VAR model, there are often too many parameters to estimate, compared to the available observations. A natural approach to overcome overparametrization is via variable selection to produce parsimonious and sparse VAR models. The introduction of networks operationalized as graphical VAR models presents a convenient framework to achieve parsimony while providing explainable interactions in multivariate time series (Ahelegbey et al., 2016a).

The concept adopted in this paper places our contribution within the literature on detection of changes in multivariate time series and specifically to Bayesian turning point models (Jochmann et al., 2010; Koop and Potter, 2007, 2009), turning point network models (Barnett and Onnela, 2016; Grzegorczyk et al., 2011; Lèbre et al., 2010; Xuan and Murphy, 2007), high dimensional Bayesian models (Ahelegbey et al., 2016b; Gruber and West, 2017; Koop et al., 2019), and the application of graphical models to cope with overffiting issues arising in high dimensional models (see Ahelegbey et al., 2016a,b; Corander and Villani, 2006; Gruber and West, 2017; Paci and Consonni, 2020). Although there has been substantial progress in modeling non-homogeneous structure of dependence among random variables, scalability to high dimensional models and large data problems remains an open issue. In this paper, we adopt a specification closely related to the Bayesian turning point model of Jochmann et al. (2010), the changing dependency structure of Xuan and Murphy (2007), and extension of the Bayesian graphical VAR model of Ahelegbey et al. (2016a) to allow for structural changes.

Several techniques for estimating turning point locations have dominated the literature on Bayesian solutions to multiple turning point problems. Prominent among such techniques are the Markov chain Monte Carlo (MCMC) and Gibbs sampling algorithms (Barry and Hartigan, 1993; Erdman and Emerson, 2008; Green, 1995; Western and Kleykamp, 2004) and recursive dynamic programming algorithms (Fearnhead, 2006; Fearnhead and Liu, 2007; Ruggieri, 2013). However, turning point estimation in high dimensional models characterized by complex interactions and large datasets with many data time points present a number of inferential and computational challenges. In such settings, standard MCMC-based techniques

usually suffer from slow mixing and high computational cost per MCMC iteration. We therefore adopt a modified version of the Bayesian sequential turning point algorithm of Ruggieri and Antonellis (2016), that employs a recursive dynamic programming scheme for multiple turning point detection problems. This scheme proves to be very effective in inferring the number and timing of the turning points, reducing the computational burden of the inference problem, especially when dealing with large data sets.

We apply our proposed model to study the equities market by considering the 15 major stock market indices, including G10 countries. The dataset consists of daily prices from Bloomberg, covering January 2000 to October 2020. The empirical application examines: 1) the turning points in the global equity market; and 2) compares the Covid-19 induced interconnectedness with that of the global financial crisis, to identify similarities and the most central market for spillover propagation.

The paper is organized as follows: Section 2 presents the piece-wise network VAR model and discuss the Bayesian estimation. Section 3 presents a description of the data and report the results in Section 4. Section 5 concludes the paper.

2. A Bayesian Graphical Piece-Wise Vector Autoregression

2.1. Piece-Wise VAR Model

Let $Y_t = (Y_{1,t}, \ldots, Y_{n,t})$ be n-variable vector of return observations at time t, where $Y_{i,t}$ is the time series of market-i at time t. Suppose there exist k turning points at $1 = \tau_0 < \tau_1 < \tau_2 < \ldots < \tau_k < \tau_{k+1} = T$. We represent the dynamics of Y_t as piece-wise stationary vector autoregressive (VAR) model of order p given by

$$Y_t = \sum_{s=1}^{p} B_s \; I(t < t^*) \; Y_{t-s} + U_t \tag{1}$$

$$U_t = B_0 \; I(t < t^*) \; U_t + \varepsilon_t \tag{2}$$

where p is the lag order, $t^* \in [\tau_{l-1}, \tau_l]$, for $l = 1, \ldots, k+1$, B_s is $n \times n$ matrix of coefficients with $B_{ij|s}$ measuring the effect of $Y_{j,t-s}$ on $Y_{i,t}$, $I(a)$ denotes the indicator function that takes value 1 if a is true and 0 otherwise, U_t is a vector independent and identically normal residuals with covariance matrix Σ_u, B_0 is a zero diagonal matrix that records the contemporaneous effect of shocks, and ε_t is a vector of orthogonalized disturbances with covariance matrix Σ_ε. From (2), the Σ_u can be expressed in terms of B_0 and Σ_ε as

$$\Sigma_u \;=\; (I - B_0)^{-1} \Sigma_\varepsilon (I - B_0)^{-1'} \tag{3}$$

2.2. Network Models

Following Ahelegbey et al. (2016a), equation (1) can be operationalize a network model, where the variables in Y are defined by nodes joined by a set of links, describing the statistical relationships between a pair of variables. The introduction of networks in VAR models helps to interpret the serial, temporal and contemporaneous relationships in a multivariate time series. To analyze (1) and (2) through networks, we assign to each coefficient in B_s a corresponding latent indicator in $G_s \in \{0,1\}^{n \times n}$, such that for $i, j = 1, \ldots, n$, and $s = 0, 1, \ldots, p$:

$$B_{ij|s} = \begin{cases} 0 & \text{if} \quad G_{ij|s} = 0 \quad \Longrightarrow \quad Y_{j,t-s} \not\rightarrow Y_{i,t} \\ \beta_{ij} \in \mathbb{R} & \text{if} \quad G_{ij|s} = 1 \quad \Longrightarrow \quad Y_{j,t-s} \rightarrow Y_{i,t} \end{cases} \tag{4}$$

where $Y_{j,t-s} \not\to Y_{i,t}$ means that Y_j does not influence Y_i at lag s, including $s = 0$, which correspond to contemporaneous dependence.

Let $B^* = \sum_{s=0}^{p} B_k$ and $G^* = \sum_{s=0}^{p} G_k$. Following (4), we define two zero diagonal matrices $A \in \{0,1\}^{n\times n}$ and $A^w \in \mathbb{R}^{n\times n}$, whose ij-th element is given by:

$$A_{ij} = \begin{cases} 0, & \text{if } G^*_{i,j} = 0 \\ 1, & \text{otherwise} \end{cases}, \qquad A^w_{ij} = \begin{cases} 0, & \text{if } B^*_{i,j} = 0 \\ B^*_{i,j} & \text{otherwise} \end{cases} \tag{5}$$

where A_{ij} specifies that $Y_j \to Y_j$ exist if there is a contemporaneous or lagged directed link from Y_j to Y_i. A^w_{ij} specifies the weights of such a relationship obtained as a sum of the estimated contemporaneous and lagged coefficients. The correspondence between (G, B) and (A, A^w) is such that the former captures the short-run dynamics in Y_t while the latter can be viewed as long-term direct relationships when $Y_t = Y_{t-1} = \ldots = Y_{t-p}$. Defining a sparse structure on (G, B) induces parsimony of the short-run model and sparsity on the long-run relationship matrices (A, A^w).

2.3. Bayesian Estimation of A Piece-Wise Network VAR

Following standard application, we select the appropriate lag order of the VAR via a Bayesian information criterion (BIC). Thus, the parameters left to estimate in a piece-wise network VAR are $(k, V_{\tau,k}, G_{1:k}, B_{1:k}, \Sigma_{\varepsilon,1:k})$, where k is the number of turning points, $V_{\tau,k} = (\tau_1, \tau_2, \ldots, \tau_k)$ is the the turning point locations, $G_{1:k} = \{G^{(1)}, \ldots, G^{(k+1)}\}$ is the collection of network graphs over the segments, $B_{1:k} = \{B^{(1)}, \ldots, B^{(k+1)}\}$ is the collection coefficient matrices over the segments, and $\Sigma_{\varepsilon,1:k} = \{\Sigma^{(1)}_{\varepsilon}, \ldots, \Sigma^{(k+1)}_{\varepsilon}\}$ is the collection of error covariance matrices over segments. Estimating these parameters jointly is a challenging problem and a computationally intensive exercise. We complete the Bayesian formulation with prior specification and posterior approximations to draw inference on the model parameters.

2.3.1. Prior Specification

We specify the prior distributions over $(k, V_{\tau,k}, G_{1:k}, B_{1:k}, \Sigma_{\varepsilon,1:k})$ as follows:

$$k \sim \mathcal{U}(0, k_{\max}), \qquad V_{\tau,k} \sim \mathcal{U}(1, T), \qquad [B^{(k)}_{ij} | G_{ij} = 1] \sim \mathcal{N}(0, \eta),$$
$$G^{(k)}_{ij} \sim \text{Ber}(\pi_{ij}), \qquad \Sigma^{-1(k)}_{\varepsilon} \sim \mathcal{W}(\delta, \Lambda_0)$$

where $k_{\max}, \eta, \pi_{ij}, \delta$, and Λ_0 are hyper-parameters.

The specification for k is a discrete uniform prior on the set $\{0, \ldots, k_{\max}\}$, with density

$$P(k) = \frac{1}{k_{\max} + 1} \mathbf{1}_{\{k \in [0, k_{\max}]\}} \tag{6}$$

The choice of the discrete uniform prior is relatively non-controversial since it is similar to the truncated Poisson in (Grzegorczyk et al., 2011; Nobile and Fearnside, 2007).

We consider $\tau_1, \ldots, \tau_k$ as order statistics and define $d_\tau = \tau_l - \tau_{l-1}$ as the distance between successive turning points. We consider $V_{\tau,k}$ to be uniformly distributed on $[1, T]$ with density

$$P(V_{\tau,k} | k) = \frac{1}{N_k}, \qquad N_k \approx \binom{T_d}{k} \tag{7}$$

where $T_d = T - d_\tau$, $\tau_0 = 1$ and $\tau_{k+1} = T$, N_k is a normalizing constant and $\binom{a}{b}$ denotes a binomial coefficient indexed by a and b. The motivation for this prior is to discourage short segments and to encourage a priori an equal spacing of the turning points. Also it shows that close observations are likely to belong to the same segment.

The specification for B_{ij} conditional on G_{ij} follows a normal distribution with zero mean and variance η. Thus, relevant explanatory variables that predict a response variable must be associated with coefficients different from zero and the rest (representing not-relevant variables) are restricted to zero. We consider G_{ij} as Bernoulli distributed with π_{ij} as the prior probability. We assume Σ_ε^{-1} is Wishart distributed with prior expectation $\frac{1}{\delta}\Lambda_0$ and $\delta > n$ the degrees of freedom parameter.

2.3.2. Posterior Approximation

Let $Z_t = (Y_t', Y_{t-1}', \ldots, Y_{t-p}')'$ be a vector of contemporaneous and lagged observations, and denote with $Z_{1:h} = (Z_1, \ldots, Z_h)$ be an $h \times m$ collection of Z_t over a window of length h, where $m = n(p+1)$. For some lag order $\hat{p}$, and under the assumption that $Z_{1:h} \sim \mathcal{N}(0, \Sigma)$, the likelihood function is given by

$$P(Z_{1:h}|\Sigma) = (2\pi)^{-\frac{mh}{2}} \ |\Sigma|^{-\frac{h}{2}} \ \text{etr}\Big(-\frac{1}{2}\Sigma^{-1}\hat{S}\Big) \tag{8}$$

where $\text{etr}(\cdot)$ is the exponential of the standard trace function, $\hat{S}$ is the sample sum of squared matrix of dimension m. It can be shown that Σ contains the structural parameters (B, Σ_ε). Under the assumption that Σ is inverse-Wishart distributed, $P(\Sigma) \sim \mathcal{IW}(\nu, \Lambda)$, with prior expectation $\frac{1}{\nu}\Lambda$ and $\nu > m$ degrees of freedom, we follow the Bayesian framework of Geiger and Heckerman (2002) to integrate out the structural parameters analytically, thus, obtaining a marginal likelihood function given by

$$P(Z|h) \ = \ \frac{(\pi)^{-\frac{mh}{2}}(\nu)^{\frac{m\nu}{2}}}{(\nu+h)^{\frac{m}{2}(\nu+h)}} \prod_{i=1}^{m} \frac{\Gamma\Big(\frac{\nu+h+1-i}{2}\Big)}{\Gamma\Big(\frac{\nu+1-i}{2}\Big)} |\bar{\Sigma}|^{-\frac{1}{2}(\nu+h)} \tag{9}$$

where $\bar{\Sigma} = (\Lambda + \hat{S})/(\nu + h)$ is the posterior covariance matrix. Clearly, we can notice that h controls the window size which is related to the turning point locations. From the above representation, we notice that except for $\bar{\Sigma}$ whose computation depends on the observed data, the rest can be pre-computed for different values of h, $1 \leq h \leq T$ with $\nu = m + 2$.

This allows us to apply an efficient sampling algorithm to sample the model parameters in blocks. The algorithm proceeds as follows:

1. Sample $[k, V_{\tau,k}|Y, \hat{p}]$ following Ruggieri and Antonellis (2016) by
   (a) Sample k from the marginal distribution: $[k|Y]$
   (b) Recursively sample $V_{\tau,k}$ from the conditional distribution: $[V_{\tau,k}|k, Y]$
2. Sample $[G_0, G_{1:\hat{p}}, B_0, B_{1:\hat{p}}, \Sigma_\varepsilon|Y, \hat{p}, k, V_{\tau,k}]$ by
   (a) Sample via a Metropolis-within-Gibbs $[G_0, G_{1:\hat{p}}|Y, \hat{p}, k, V_{\tau,k}]$ by
      i. Sampling from the marginal distribution: $[G_{1:\hat{p}}|Y, \hat{p}, k, V_{\tau,k}]$
      ii. Sampling from the conditional distribution: $[G_0|Y, \hat{p}, G_{1:\hat{p}}, k, V_{\tau,k}]$
   (b) Sample from $[B_0, B_{1:\hat{p}}, \Sigma_\varepsilon|Y, \hat{G}_0, \hat{G}_{1:\hat{p}}, \hat{p}, k, V_{\tau,k}]$ by iterating the following steps:

i. Sample $[B_{i,\pi_i|1:\hat{p}}|Y, \hat{G}_{1:\hat{p}}, \hat{G}_0, B_0, \Sigma_\varepsilon] \sim \mathcal{N}(\hat{B}_{i,\pi_i|1:\hat{p}},\ D_{\pi_i})$ where

$$\hat{B}_{i,\pi_i|1:\hat{p}} = \sigma_{u,i}^{-2} D_{\pi_i} Z'_{\pi_i} Y_i, \qquad D_{\pi_i} = (\eta^{-1} I_{d_z} + \sigma_{u,i}^{-2} Z'_{\pi_i} Z_{\pi_i})^{-1} \tag{10}$$

where $Z_{\pi_i} \in Z$ corresponds to $(\hat{G}_{y_i,z_\pi|1:\hat{p}} = 1)$, $\sigma_{u,i}^2$ is the i-th diagonal element of $\hat{\Sigma}_u = (I - \hat{B}_0)^{-1} \hat{\Sigma}_\varepsilon (I - \hat{B}_0)^{-1'}$, and d_z is the number of covariates in Z_{π_i}.

ii. Sample $[B_{i,\pi_i|0}|Y, \hat{G}_0, \hat{G}_{1:\hat{p}}, B_{1:\hat{p}}, \Sigma_\varepsilon] \sim \mathcal{N}(\hat{B}_{i,\pi_i|0}, Q_{\pi_i})$ where

$$\hat{B}_{i,\pi_i|0} = \sigma_{\varepsilon,i}^{-2} Q_{\pi_i} \hat{U}'_{\pi_i} \hat{U}_i, \qquad Q_{\pi_i} = (\eta^{-1} I_{d_u} + \sigma_{\varepsilon,i}^{-2} \hat{U}'_{\pi_i} \hat{U}_{\pi_i})^{-1} \tag{11}$$

where $\hat{U} = Y - Z\hat{B}'_{1:\hat{p}}$, $\hat{U}_{\pi_i} \in \hat{U}_{-i}$ is the contemporaneous predictors of $\hat{U}_i$ that corresponds to $(\hat{G}_{y_i,y_\pi|0} = 1)$, and d_u is the number of covariates in U_{π_i}

iii. Sample $[\Sigma_\varepsilon^{-1}|Y, \hat{G}_{1:\hat{p}}, \hat{G}_0, B_{1:\hat{p}}, B_0] \sim \mathcal{W}(\delta + N,\ \Lambda_N)$ where

$$\Lambda_N = \Lambda_0 + (\hat{U} - \hat{U}\hat{B}'_0)'(\hat{U} - \hat{U}\hat{B}'_0) \tag{12}$$

A detailed description on how to sample the parameters is available in Appendix A.

3. Data Description

Our study makes use of daily data from Bloomberg, covering between January 2000 to October 2020, and includes 15 major stock market indices, including all G10 economies. We consider only one index per country, which typically contains the stock prices of the largest companies listed in the nation's largest stock exchange. The countries can be grouped into three regions: the Americas (Brazil, Canada, and the United States), Asia-Pacific (Australia, China, Hong Kong, India, Japan, and South Korea), and Europe (France, Germany, Italy, Russia, Spain, and the United Kingdom). A description of the market indices chosen for the selected countries is presented in Table 1.

Region	No.	Country	Code	Description	Index
Americas	1	Brazil	BR	Brazil Bovespa	IBOV
	2	Canada	CA	Canada TSX Comp.	SPTSX
	3	United States	US	United States S&P 500	SPX
Asia-Pacific	4	Australia	AU	Australia ASX 200	AS51
	5	China	CN	China SSE Comp.	SHCOMP
	6	Hong Kong	HK	Hong Kong Hang Seng	HSI
	7	India	IN	India BSE Sensex	SENSEX
	8	Japan	JP	Japan Nikkei 225	NKY
	9	Korea	KR	South Korean KOSPI	KOSPI
Europe	10	France	FR	France CAC 40	CAC
	11	Germany	DE	Germany DAX 30	DAX
	12	Italy	IT	Italy FTSE MIB	FTSEMIB
	13	Russia	RU	Russia MOEX	IMOEX
	14	Spain	ES	Spain IBEX 35	IBEX
	15	United Kingdom	UK	UK FTSE 100	UKX

Table 1: Description of stock market indices of countries classified according to regions.

We report in Figure 1 the daily series of closing prices on a logarithmic scale. We scale the prices to a zero mean and unit variance and add the absolute minimum value of each series to avoid negative outcomes. This standardizes the scale of measurement for the different series. The figure shows that over the past two decades, global financial markets have experienced

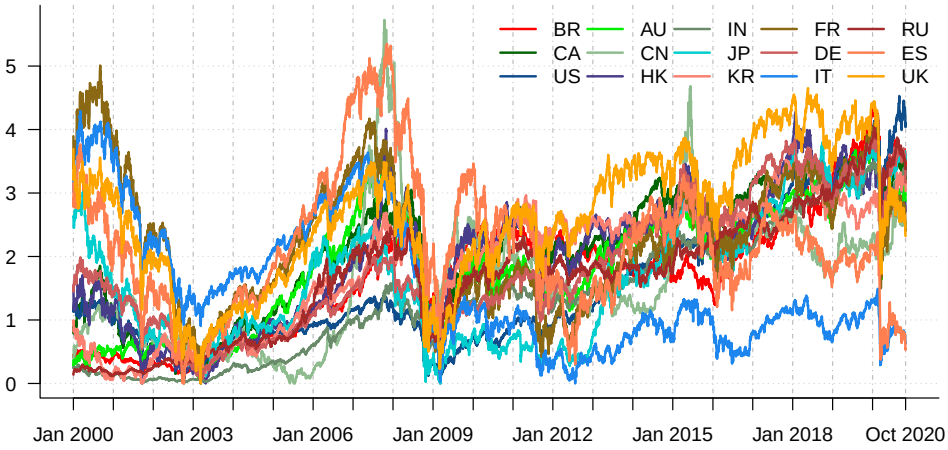

Figure 1: Daily closed prices of major stock market indices (January 3, 2000 – October 30, 2020).

several catastrophic events within and across different markets. Among these events is 1) the dotcom "tech" induced crisis of 2000–2003 which was fuelled by the adoption of the internet in the late 1990s, triggering inflated stock prices that gradually went downhill and disrupted global market operations; 2) the global financial crisis of 2007–2009 which was triggered by the massive defaults of sub-prime borrowers in the US mortgage market; 3) the European sovereign debt crisis of 2010–2013 which emanated from the inability of a cluster of EU member states to repay or refinance their sovereign debt and bailout heavily leveraged financial institutions without recourse to third party assistance; and 4) the distress to world economy and global financial markets caused by the novel coronavirus pandemic in 2020.

Country	Code	Min	Max	Mean	SD	Skew	Ex.Kurt
Brazil	BR	-15.993	28.824	0.047	1.861	0.318	16.057
Canada	CA	-13.176	11.295	0.016	1.124	-0.898	16.780
United States	US	-12.765	10.957	0.018	1.244	-0.362	10.849
Australia	AU	-10.203	6.766	0.014	1.014	-0.707	8.524
China	CN	-9.256	9.401	0.019	1.528	-0.271	5.324
Hong Kong	HK	-13.582	13.407	0.016	1.446	-0.087	7.600
India	IN	-14.102	15.990	0.046	1.471	-0.247	9.155
Japan	JP	-12.111	13.235	0.009	1.450	-0.358	6.699
Korea	KR	-12.805	11.284	0.025	1.529	-0.456	6.451
France	FR	-13.098	10.595	0.003	1.437	-0.213	6.174
Germany	DE	-13.055	10.797	0.015	1.484	-0.163	5.652
Italy	IT	-18.541	10.874	-0.012	1.530	-0.570	8.949
Russia	RU	-20.657	25.226	0.073	2.066	-0.063	14.146
Spain	ES	-15.151	13.484	-0.008	1.466	-0.309	7.796
United Kingdom	UK	-11.512	9.384	-0.001	1.191	-0.329	7.697

Table 2: Statistics of daily returns for stock market indices over the sample period.

We compute daily returns as the log differences of successive daily closing prices, that is,

$Y_{i,t} = 100\,(\log C_{i,t} - \log C_{i,t-1})$, with $C_{i,t}$ the daily closing price of market i on trading day t. Table 2 reports a set of summary statistics for the index returns over the sample period. The table shows that almost all index returns have a near-zero mean and a relatively high standard deviation. The highest standard deviations, indicating individual market volatilities, are those of the emerging markets of Russia and Brazil. Almost all the return indices exhibit fairly symmetric behaviour, i.e., they are characterized mostly by small but consistent positive gains and, occasionally, large negative returns. The excess kurtosis varies between 5.32 (China) and 16.78 (Canada), which confirms the stylized facts of leptokurtic behavior of daily return series.

4. Empirical Findings

We begin by studying the turning points in the equity market interconnectedness over the sample period. We characterize the dynamics of the connectedness via a yearly rolling windows of 240 trading days. We monitor the daily changes in the interconnectedness by setting the increments between successive rolling windows to one day. Thus, we set the first window of our study from January 28, 1999, to January 3, 2000, followed by January 29, 1999, to January 4, 2000; the last window is from November 21, 2019, to October 30, 2020. In total, we consider 5318 rolling windows. We select the appropriate lag of the VAR via a Bayesian information criterion (BIC) for different lag orders ($p \in \{1, \ldots, 7\}$). The optimal lag order according minimum BIC score is $p = 1$.

We report in Figure 2 the plot of rolling-window Net-Density and the posterior probability of a turning point for each day between January 3, 2000 to October 30, 2020. The figure shows

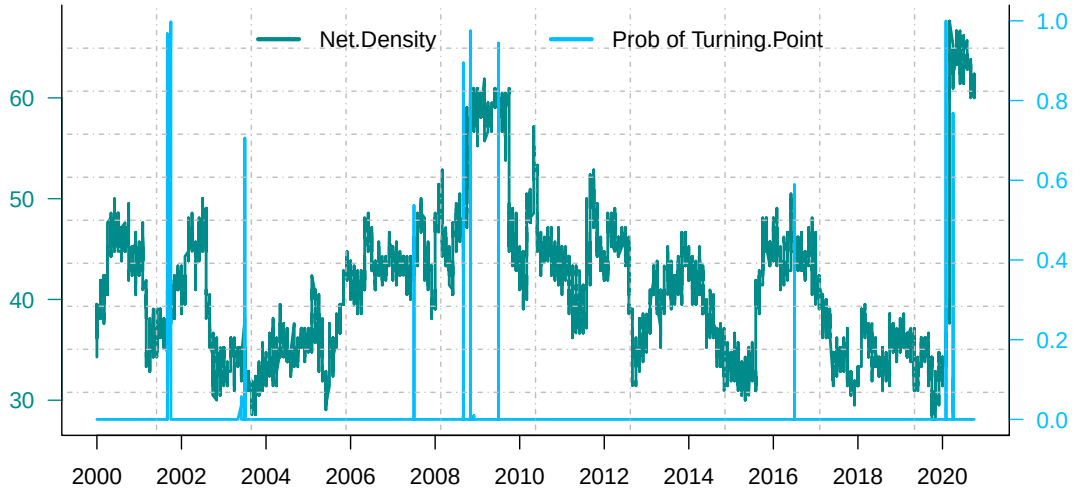

Figure 2: A rolling-window Net-Density and Posterior probability of turning points.

that the network density of the COVID-19 period is much greater than any period of market crisis in the last 20 years, and this include the period of the dotcom "tech" induced crisis of 2000–2003, the global financial crisis (GFC) of 2007–2009, and the European sovereign debt crisis of 2010–2013. The spike in the network density after February 2020 is typified by the fear and panic that greeted the global financial market, and thus, intensifying sell-off of assets. The increased interconnectedness during the pandemic beyond the level recorded during the GFC suggest stronger evidence of contagion in the coronavirus pandemic than during the financial and eurozone crisis.

4.1. Turning Points in Global Equity Markets

For clarity, we extract the turning point dates, as they emerge from Figure 2. Table 3 lists the turning point dates with their posterior probabilities and possible financial market events that characterize the identified dates.

	Dates	Probability	Financial Market Event
1	11/09/2001	0.967	September 11 Effect
2	01/10/2001	0.997	Turn-around in Financial markets
3	08/07/2003	0.706	Turn-around after SARS induced crisis
4	23/07/2007	0.528	Panic in the asset-backed commercial paper market
5	15/09/2008	0.896	Bankruptcy of Lehman Brothers
6	06/11/2008	0.976	IMF prediction of deep recession
7	07/07/2009	0.945	End of the great recession
8	12/07/2016	0.584	Rising oil prices and Aftermath of Brexit
9	21/02/2020	0.999	Beginning of Covid-19 induced global stock market crash
10	08/04/2020	0.921	End of Covid-19 induced global stock market crash

Table 3: Turning point dates with their posterior probabilities and possible financial market events.

The first turning point (event #1) in financial market over the past two decade is the September 11, 2001 attack that led to one of the largest single-day point decline in major markets. This was followed by a turn-around in at the beginning of October 2001 (event #2).

The timeline of the Severe Acute Respiratory Syndrome (SARS) outbreak shows that the illness first appeared in Guangdong Province, China in November 2002 and spread to 37 countries. This affected the Asian financial market and began to affect stock market integration around early 2003. The World Health Organisation (WHO) database shows that the SARS infection period was from 16/11/2002 – 05/07/2003 (see World Health Organization, 2003). Thus, the third turning point (event #3) captures the turn-around in financial market as a result of WHO's declaration that SARS outbreaks have been contained worldwide.

The fourth turning point (event #4) marks the contraction in the asset-backed commercial paper (ABCP) market that began in late July 2007, which triggered fears and panic across the financial market. As documented by Covitz et al. (2013) and in Financial Crisis Inquiry Commission (2011), the collapse of the ABCP market played a central role in transforming concerns about the credit quality of mortgage-related assets into a global financial crisis. Early July 2007 also experienced the collapse of two Bear Stearns hedge funds that had speculated heavily in mortgage-backed securities.

The fifth turning point (event #5) marks September 15, 2008 when stock markets experienced the worst sell-off in the last 20 years. It was a Monday that followed a weekend turmoil of triple trouble. That is, Lehman Brothers (the fourth-largest U.S. investment bank at the time) filed for Chapter 11 bankruptcy protection; Merrill Lynch was acquired by Bank of America; and the American International Group (AIG - the world's largest insurance company) presented an unprecedented request for short-term financing from the Federal Reserve. According to the Financial Crisis Inquiry Commission (2011), the risk exposures of AIG are concentrated among the largest international banks (both US and European) across a wide array of product types (bank lines, derivatives, securities lending, etc.). Thus, AIG's failure could trigger significant counterparty losses to these firms. The fears and panic across financial markets led to increased interconnectedness which amplified the shocks, affecting a broader aspect of the US financial system and many other correlated markets and economies.

By the end of October 2008, many advanced economies like the US, Europe and Japan were already facing their deepest recession since the 1930s. With the global financial market in turmoil, producers and consumers were losing confidence in the financial system. As documented in the World Economic Outlook report published on November 6th 2008 (see IMF, 2008), the IMF predicted a worldwide "deep recession" in 2009 following the deteriorated global growth of world GDP over the past month. This forecast coupled with financial conditions continued to present serious downside risks, pushing the world over the edge with reaction across major stock markets. Thus, the sixth turning point (event #6) marks the date of the IMF prediction with its effect on the global equity market.

The seventh turning point (event #7) identifies July 7th 2009 as the day that marks the beginning of global economy recovery from the great recession. In its World Economic Outlook report published on July 8th 2009 (see IMF, 2009), the IMF projected receding contractionary forces with a positive but weak recovery between 2009–2010.

Rising crude oil prices in July 2016 affected oil producing countries as well oil dependent nations, sending market participants worried about the possible impact of rising crude oil prices on global stock market activities. The period also coincides with the aftermath of the Brexit which saw Britain voting to exit the EU in June 2016. The uncertainty surrounding the Brexit had significant effect on many investors thereby altering financial market activities across the globe. The failure of the Bank of England to ease the shocks that followed the Brexit vote also contribute to a mild turning point (i.e. event #8).

Discussions of the first Coronavirus case dates back to mid-November 2019. A global pandemic was triggered when the severity and scale of the impact of the novel coronavirus led to what can be best described as "hibernation" of world activities, i.e., a temporary sleep or "artificial coma". February 21st 2020 (event #9) marked the day Covid-19 outbreak began to affect Europe and the U.S., plunging many stock markets into turmoil. Despite its impact, the GFC is incomparable to the Covid-19 outbreak in terms of the scale and magnitude of its effects. The uncertainty at the onset of latter was accompanied by the existential threat from which many markets may not recover in the sense that it could cripple if not wipe out nations and economies completely. This assertion is evidence by the fact that it recorded the fastest fall in global stock markets (see Figure 1). Unlike any of the past crises, within just a month of reported coronavirus cases in Europe and the US, major national indices began to record their worst ever historical prices in history.

The last turning point (event #10) mark the beginning of financial market recovery from the Covid-19 outbreak. Although, the global stock market is in a recovery phase, major world economies are currently in a recession or depression.

4.2. Dynamic Interconnectedness In Global Equity Markets

We analyze the dynamic nature of the interconnectedness among the major stock markets to assess which markets over the past two decades. Using the turning point dates, we divide the sample into four sub-periods of tranquil and turbulent times: (03/01/2000 – 12/09/2008), (15/09/2008 – 06/07/2009), (07/07/2009 – 20/02/2020) and (21/02/2020 – 30/10/2020). We report in Figure 3 the network topology over the sub-periods. Each network is represented with color-coded links and nodes. Red-links indicate negative weights and green-links denote positive weights. Red-color nodes represent American markets, blue-nodes for European markets, and green-nodes for markets in Asia-Pacific countries. The size of the nodes is proportional to their hub scores.

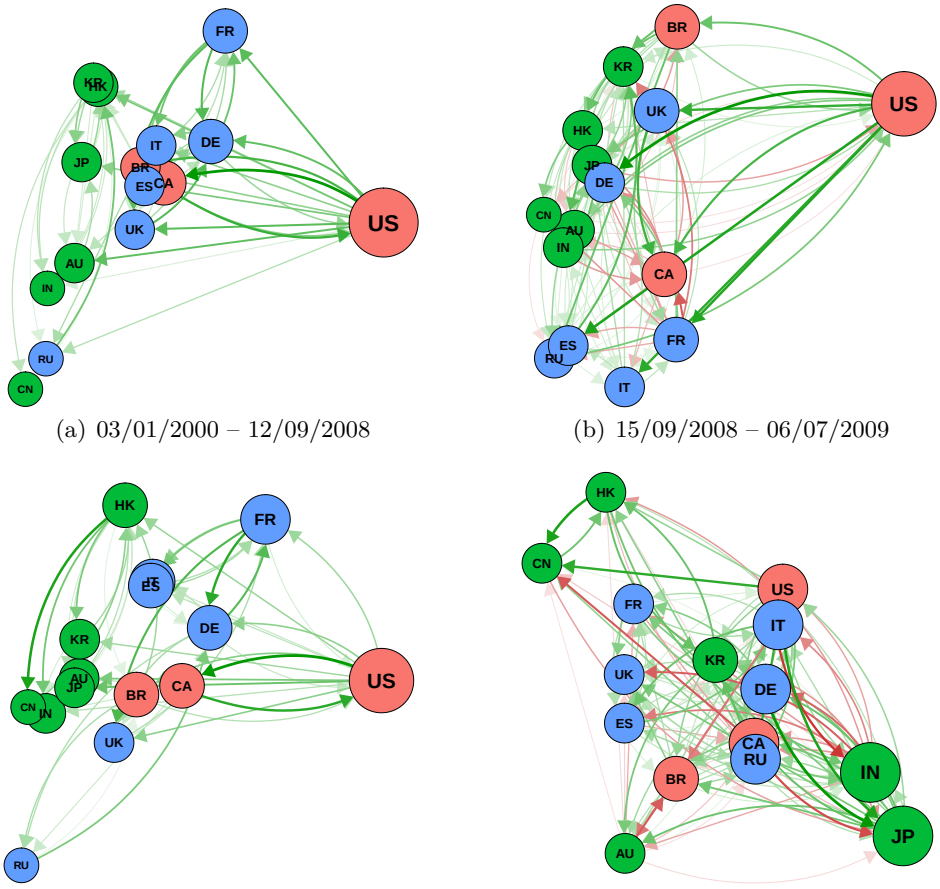

(a) 03/01/2000 – 12/09/2008

(b) 15/09/2008 – 06/07/2009

(c) 07/07/2009 – 20/02/2020

(d) 21/02/2020 – 30/10/2020

Figure 3: Sub-period Interconnectedness. Red nodes represent America markets, blue for European, and green for Asia-Pacific. The size of the nodes are weighted out-degree. Red links denote negative effects and green for positive interactions. The node position is based on eigendecomposition of the networks.

The figure provides strong evidence of clustering among the markets. More importantly, the Asian-Pacific markets (green-nodes) seem to move together, likewise, the European markets (blue-nodes) due to similarities in underlying market conditions. The US, however, appears separated from the others most of the time, as the rest of the American markets (red-nodes) are usually closer to the European ones. We notice that the US is usually the biggest sized node and strongly positively connected to the rest of the markets. Based on the node sizes, the US appears to be the most influential in almost all the sub-periods except 21/02/2020 – 30/10/2020, where Japan seems to dominate.

We compare the sub-period networks in terms of average degree, density, clustering coefficient, and average path length (see Appendix B for a description of these network statistical metrics). Table 4 shows that network statistics extracted for the four sub-period connectivity structures. We notice that two sub-periods record tranquil (non-crisis) conditions (i.e., 03/01/2000 – 12/09/2008 and 07/07/2009 – 20/02/2020), while the other two (15/09/2008 – 06/07/2009, and 21/02/2020 – 30/10/2020) experienced stressful conditions. The tranquil periods are characterized by relatively low average degree of interconnectedness, lowe density and clustering index, and a relatively high average path length. This suggests a lower degree

No.	Date Interval	Average Degree	Density	Clustering Coefficient	Average Path Length
1	03/01/2000 – 12/09/2008	4.000	28.571	0.597	1.903
2	15/09/2008 – 06/07/2009	8.133	58.095	0.760	1.419
3	07/07/2009 – 20/02/2020	4.133	29.524	0.532	2.171
4	21/02/2020 – 30/10/2020	8.800	62.857	0.824	1.371

Table 4: The network statistics for sub-period interconnectedness graphs.

of equity market integration before and after the global financial crisis. It also shows that in the event a shock to a major market or a group of major markets, these shocks will take a much longer time to propagate to other markets to cause a systemic breakdown.

The turbulent periods, on the other hand, are characterized by relatively high average degree of interconnectedness, high density and clustering index, and a relatively low average path length. The lower average path length shows that it takes a relatively shorter time for a shock to a major market or a group of major markets to propagate to other markets, leading to a systemic breakdown. The network statistics of 15/09/2008 – 06/07/2009 and 21/02/2020 – 30/10/2020 periods shows that stock market integration during the GFC is strikingly similar to the behavior exhibited most recently at the height of the Coronavirus pandemic in 2020. More importantly, the spikes in the network density at onset of both crisis periods (see Figure 2) indicate elevated levels of unusualness in stock markets with a rise in volatility and market co-movements.

4.3. Global Financial Crisis vs Covid-19 Outbreak

We compare the interconnectedness of markets during the GFC and the Covid-19 outbreak. For this comparison, we extract the intersection and differences between the networks. Figure 4 presents the similarity and difference between the structure of interconnectedness during the GFC and Covid-19 sub-periods. Figure 4(a) depicts the network links during the GFC but not in the Covid-19 period. Figure 4(b) display the network links common to both periods, and Figure 4(c) shows only links in the Covid-19 period but not present during the GFC. Overall, we found 77 common connections between both networks. The GFC recorded 44 extra links that not present in the Covid-19 network, and the latter also report 54 new connections that was not in existence during the financial crisis. Surprisingly, majority of the new stock market connections center around Japan, Germany and India, whereas the GFC period centered around the US.

We now turn our attention to assess and compare the most critical (or central) market to during what appears to be the two most severe equity market crisis over the last two decades. Table 5 reports the summary of the centrality ranking of the most influential markets over the two crisis sub-periods. The table shows the top three transmitters of spillover propagation during the GFC are the US, UK and France, while the top three receivers of shocks during the period were Canada, Germany and France. During the Covid-19 outbreak, this most central markets for transmitting shocks are Japan, India and the US, while Japan, Australia, and Russia ranks high at the receiving end of shocks. Thus, not only has the structure of the nature of interconnectedness changed over the two crisis, but the most central markets for spillover propagation has also changed in recent times.

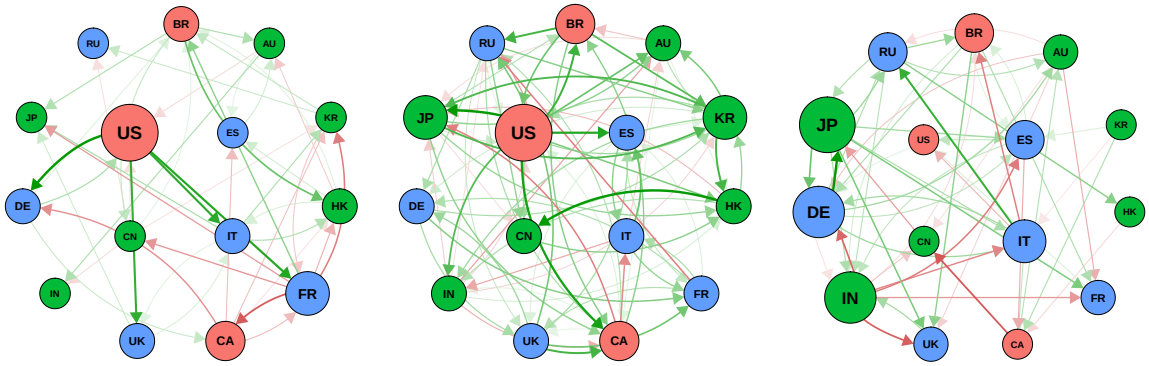

(a) $GFC \cap COVID^c$ (# 44) (b) $GFC \cap COVID$ (# 77) (c) $GFC^c \cap COVID$ (# 54)

Figure 4: Comparing the Global Financial Crisis (GFC) and Covid-19 outbreak Network. Red nodes represent America markets, blue for European, and green for Asia-Pacific. The size of the nodes are weighted out-degree. Red links denote negative effects and green for positive interactions. The number in parenthesis signifies the total links in each network. Note: A^c - Complement of A.

Rank	**GFC (2008–2009)**		**COVID (2020)**	
	Hub	Auth	Hub	Auth
1	US (0.798)	CA (0.383)	JP (0.432)	JP (0.346)
2	UK (0.265)	DE (0.359)	IN (0.412)	AU (0.308)
3	FR (0.256)	FR (0.328)	US (0.346)	RU (0.283)
4	BR (0.249)	ES (0.319)	IT (0.331)	CA (0.280)
5	CA (0.228)	IT (0.292)	DE (0.288)	IN (0.279)
6	IT (0.182)	JP (0.281)	RU (0.283)	KR (0.272)
7	KR (0.161)	UK (0.252)	CA (0.275)	DE (0.263)
8	HK (0.101)	HK (0.238)	KR (0.228)	UK (0.252)
9	JP (0.098)	KR (0.235)	BR (0.190)	BR (0.251)
10	DE (0.097)	BR (0.221)	FR (0.146)	CN (0.246)
11	AU (0.092)	IN (0.208)	HK (0.134)	ES (0.240)
12	IN (0.074)	AU (0.190)	UK (0.127)	FR (0.222)
13	RU (0.068)	RU (0.157)	ES (0.124)	HK (0.209)
14	ES (0.063)	CN (0.133)	AU (0.119)	US (0.187)
15	CN (0.049)	US (0.068)	CN (0.040)	IT (0.182)

Table 5: Centrality ranking during Global Financial Crisis and Covid-19 Pandemic.

5. Conclusion

This paper studies the nature of turning point in financial equity markets. We propose a Bayesian technique for turning point detection in a piece-wise network vector autoregressive model that approximates the interconnectedness among stock market returns. The empirical application examines turning points in global equity market over the past two decades. We also compare the Covid-19 induced interconnectedness with that of the global financial crisis to identify similarities and the most central markets for spillover propagation.

Our proposed approach proves to be effective in identifying financial market turning points in relevant periods, like the September 11 attack of 2001, the turn-around after SARS induced crisis in 2003, the panic in the asset-backed commercial paper market in 2007, the Bankruptcy of Lehman Brothers in 2008, the beginning and the end of the 2008–2009 great recession,

the rising oil prices and aftermath of Brexit in 2016, and the beginning and end of Covid-19 induced global stock market crash in 2020. We document a significant change in the structure of stock market integration during the global financial crisis and the Covid-19 outbreak. The result shows that the Covid-19 induced market interconnections record the highest density, suggesting stronger evidence of spillovers and contagion in the Covid-19 outbreak than during the global financial crisis.

References

Ahelegbey, D. F., M. Billio, and R. Casarin (2016a). Bayesian Graphical Models for Structural Vector Autoregressive Processes. *Journal of Applied Econometrics 31*(2), 357–386.

Ahelegbey, D. F., M. Billio, and R. Casarin (2016b). Sparse Graphical Vector Autoregression: A Bayesian Approach. *Annals of Economics and Statistics 123/124*, 333–361.

Bai, J. (2000). Vector Autoregressive Models with Structural Changes in Regression Coefficients and in Variance-Covariance Matrices. *Annals of Economics and Finance 1*(2), 303–339.

Barigozzi, M. and C. Brownlees (2019). NETS: Network Estimation for Time Series. *Journal of Applied Econometrics 34*(3), 347–364.

Barnett, I. and J.-P. Onnela (2016). Change Point Detection in Correlation Networks. *Scientific Reports 6*, 18893.

Barrat, A. and M. Weigt (2000). On The Properties of Small-World Network Models. *The European Physical Journal B-Condensed Matter and Complex Systems 13*(3), 547–560.

Barry, D. and J. A. Hartigan (1993). A Bayesian Analysis for Change Point Problems. *Journal of American Statistical Association 88*(421), 309–319.

Basu, S. and G. Michailidis (2015). Regularized Estimation in Sparse High-dimensional Time Series Models. *The Annals of Statistics 43*(4), 1535–1567.

Battiston, S., D. Delli Gatti, M. Gallegati, B. Greenwald, and J. E. Stiglitz (2012). Liaisons Dangereuses: Increasing Connectivity, Risk Sharing, and Systemic Risk. *Journal of Economic Dynamics and Control 36*(8), 1121–1141.

Bianchi, D., M. Billio, R. Casarin, and M. Guidolin (2019). Modeling Systemic Risk with Markov Switching Graphical SUR Models. *Journal of Econometrics 210*(1), 58–74.

Billio, M., R. Casarin, and L. Rossini (2019). Bayesian Nonparametric Sparse VAR Models. *Journal of Econometrics 212*(1), 97–115.

Billio, M., M. Getmansky, A. W. Lo, and L. Pelizzon (2012). Econometric Measures of Connectedness and Systemic Risk in the Finance and Insurance Sectors. *Journal of Financial Economics 104*(3), 535 – 559.

Chib, S. (1998). Estimation and Comparison of Multiple Change-point Models. *Journal of Econometrics 86*(2), 221–241.

Cho, H. and P. Fryzlewicz (2015). Multiple Change-point Detection for High-dimensional Time Series via Sparsified Binary Segmentation. *Journal of the Royal Statistical Society: Series B (Statistical Methodology) 77*(2), 475–507.

Corander, J. and M. Villani (2006). A Bayesian Approach to Modelling Graphical Vector Autoregressions. *Journal of Time Series Analysis 27(1)*, 141–156.

Covitz, D., N. Liang, and G. A. Suarez (2013). The Evolution of a Financial Crisis: Collapse of the Asset-Backed Commercial Paper Market. *The Journal of Finance 68*(3), 815–848.

DasGupta, B. and L. Kaligounder (2014). On Global Stability of Financial Networks. *Journal of Complex Networks 2*(3), 313–354.

Diebold, F. and K. Yilmaz (2014). On the Network Topology of Variance Decompositions: Measuring the Connectedness of Financial Firms. *Journal of Econometrics 182*(1), 119–134.

Erdman, C. and J. W. Emerson (2008). A Fast Bayesian Change Point Analysis for the Segmentation of Microarray Data. *Bioinformatics 24*(19), 2143–2148.

Fearnhead, P. (2006). Exact and Efficient Bayesian Inference for Multiple Changepoint Problems. *Statistics and Computing 16*(2), 203–213.

Fearnhead, P. and Z. Liu (2007). On-line Inference for Multiple Changepoint Problems. *Journal of the Royal Statistical Society: Series B (Statistical Methodology) 69*(4), 589–605.

Financial Crisis Inquiry Commission (2011). *The Financial Crisis Inquiry Report: The Final Report of the National Commission on the Causes of the Financial and Economic Crisis in the United States*. Public Affairs.

Geiger, D. and D. Heckerman (2002). Parameter Priors for Directed Acyclic Graphical Models and the Characterization of Several Probability Distributions. *Annals of Statistics 30*(5), 1412–1440.
Gelman, A. and D. B. Rubin (1992). Inference from Iterative Simulation Using Multiple Sequences, (with discussion). *Statistical Science 7*, 457–511.
Green, P. J. (1995). Reversible Jump Markov Chain Monte Carlo Computation and Bayesian Model Determination. *Biometrika 82*(4), 711–732.
Gruber, L. F. and M. West (2017). Bayesian Forecasting and Scalable Multivariate Volatility Analysis Using Simultaneous Graphical Dynamic Models. *Econometrics and Statistics 3*, 3–22.
Grzegorczyk, M., D. Husmeier, and J. Rahnenführer (2011). Modelling Non-stationary Dynamic Gene Regulatory Processes with the BGM Model. *Computational Statistics 26*(2), 199–218.
Hautsch, N., J. Schaumburg, and M. Schienle (2015). Financial Network Systemic Risk Contributions. *Review of Finance 19*(2), 685–738.
IMF (2008). World Economic Outlook Update: Rapidly Weakening Prospects Call For New Policy Stimulus.
IMF (2009). World Economic Outlook Update: Contractionary Forces Receding But Weak Recovery Ahead.
Jochmann, M., G. Koop, and R. W. Strachan (2010). Bayesian Forecasting using Stochastic Search Variable Selection in a VAR Subject to Breaks. *International Journal of Forecasting 26*(2), 326–347.
Koop, G., D. Korobilis, and D. Pettenuzzo (2019). Bayesian Compressed Vector Autoregressions. *Journal of Econometrics 210*(1), 135–154.
Koop, G. and S. M. Potter (2007). Estimation and Forecasting in Models with Multiple Breaks. *The Review of Economic Studies 74*(3), 763–789.
Koop, G. and S. M. Potter (2009). Prior Elicitation in Multiple Change-Point Models. *International Economic Review 50*(3), 751–772.
Lèbre, S., J. Becq, F. Devaux, M. P. Stumpf, and G. Lelandais (2010). Statistical Inference of the Time-varying Structure of Gene Regulation Networks. *BMC systems biology 4*(1), 130.
Nobile, A. and A. T. Fearnside (2007). Bayesian Finite Mixtures with an Unknown Number of Components: The Allocation Sampler. *Statistics and Computing 17*(2), 147–162.
Paci, L. and G. Consonni (2020). Structural Learning of Contemporaneous Dependencies in Graphical VAR Models. *Computational Statistics & Data Analysis 144*, 106880.
Pesaran, M. H., D. Pettenuzzo, and A. Timmermann (2006). Forecasting Time Series Subject to Multiple Structural Breaks. *The Review of Economic Studies 73*(4), 1057–1084.
Qu, Z. and P. Perron (2007). Estimating and Testing Structural Changes in Multivariate Regressions. *Econometrica 75*(2), 459–502.
Ruggieri, E. (2013). A Bayesian Approach to Detecting Change Points in Climatic Records. *International Journal of Climatology 33*(2), 520–528.
Ruggieri, E. and M. Antonellis (2016). An Exact Approach to Bayesian Sequential Change Point Detection. *Computational Statistics and Data Analysis 97*, 71–86.
Western, B. and M. Kleykamp (2004). A Bayesian Change Point Model for Historical Time Series Analysis. *Political Analysis 12*, 354–374.
World Health Organization (2003). Update 95-SARS: Chronology of a Serial Killer.
Xuan, X. and K. Murphy (2007). Modeling Changing Dependency Structure in Multivariate Time Series. In *Proceedings of the 24th International Conference on Machine Learning*, pp. 1055–1062. ACM.

Appendix A. Details of Sampling Approach of the Parameters

This section provides a detailed description of the sampling approach of the parameters.

Appendix A.1. Sampling Number of Turning Points

Using Bayes rule, the posterior distribution on the number of turning points is given as:

$$\begin{aligned} P(K=k|Z) &= \frac{P(K=k)P(V_{\tau,k}|K=k)P(Z|K=k,V_{\tau,k})}{P(Z)} \\ &= \frac{1}{k_{\max}+1}\,\frac{1}{N_k}\,\frac{P(Z|K=k,V_{\tau,k})}{P(Z)} \qquad \text{(A.1)} \\ \text{where} \quad P(Z) &= \sum_K \sum_{V_{\tau,k}} P(Z|K=k,V_{\tau,k})P(K=k,V_{\tau,k}) \qquad \text{(A.2)} \end{aligned}$$

For $t = 1, \ldots, T$, we denote with $\Psi_k(1,h) = P(Z_{1:h}|K = k, V_{\tau,k})$, the density of $Z_{1:h}$ with $k > 0$ turning points defined by

$$\Psi_k(1,h) = \sum_{t<h} \Psi_{k-1}(1,t) P(Z_{t+1:h}) \tag{A.3}$$

for $h = (d_\tau + 1), \ldots, T$, where the above density for $k = 0$ is initialized by $\Psi_0(1,h) = P(Z_{1:h})$, and $d_\tau = \tau_l - \tau_{l-1}$ is the distance between two successive turning points.

Appendix A.2. Sample Turning Point Locations

Following the process of filtering recursion (see Fearnhead, 2006; Ruggieri, 2013), the posterior distribution of the first turning point is given by

$$P(\tau_1 = s|Z) = \frac{\Psi_0(1,s)\ P(Z_{s+1:T})}{\sum_{s<T} \Psi_0(1,s)\ P(Z_{s+1:T})} \tag{A.4}$$

and the posterior distribution of the first turning point is given by

$$P(\tau_k = t|\tau_{k+1}, Z) = \frac{\Psi_{k-1}(Z_{1:t})\ P(Z_{t+1:\tau_{k+1}})}{\sum\limits_{t\in[k-1,\tau_{k+1})} \Psi_{k-1}(Z_{1:t})\ P(Z_{t+1:\tau_{k+1}})} \tag{A.5}$$

Appendix A.3. Sampling The Network

Let $V_y = (y_i, \ldots, y_n)$ be the vector of indices of response variables, and $V_z = (z_1, \ldots, z_{n\hat{p}})$ the indices of the lagged observations. The network relationship from $z_\psi \in V_z$ to $y_i \in V_y$ can be represented by $(G_{y_i,z_\psi} = 1)$. Following Geiger and Heckerman (2002), the closed-form expression of the local marginal likelihood is given by

$$P(Y|G_{y_i,z_\psi}) = \frac{\pi^{-\frac{1}{2}N}\ \nu_0^{\frac{1}{2}\nu_0}}{\nu_n^{\frac{1}{2}\nu_n}} \frac{\Gamma\left(\frac{\nu_0+N-n_x}{2}\right)}{\Gamma\left(\frac{\nu_0-n_x}{2}\right)} \left(\frac{|Z'_\psi Z_\psi + \nu_0 I_{n_v}|}{|X'_i X_i + \nu_0 I_{n_x}|}\right)^{\frac{1}{2}\nu_n} \tag{A.6}$$

where $\Gamma(\cdot)$ is the gamma function, $X_i = (Y_i, Z_\psi)$, I_d is a d-dimensional identity matrix, n_ψ is the number of covariates in Z_ψ, $n_x = n_\psi + 1$, $\nu_0 > n_x$ is a degree of freedom hyper-parameter of the prior precision matrix of (Y, Z), and $\nu_n = \nu_0 + N$. Equation (A.6) indicates that only the ratio of the posterior sum of squares depend on the data. Thus, we reduce computational time by pre-computing the part of (A.6) that is independent of the data, for different values of $n_x \in [1, m]$ and for fixed $\nu_0 = m + 2$ and N. We also pre-compute the posterior of the full sum of squares matrix and extract the sub-matrices that relates to $\{Z_\psi\}$ and $\{(Y_i, Z_\psi)\}$. For computational details of the score function (see Ahelegbey et al., 2016a). See Algorithms 1 and 2 for a pseudo code of the lagged and contemporaneous network sampling steps.

For our empirical application, we set the hyper-parameters as follows: $\pi_{ij} = 0.5$ (which leads to a uniform prior on the graph space), $\eta = 100, \delta = n + 2$ and $\Lambda_0 = \delta I_n$. We set the number of MCMC iterations to sample 50,000 graphs and we ensured that the convergence and mixing of the MCMC chains are tested via the potential scale reduction factor (PSRF) of Gelman and Rubin (1992).

Algorithm 1 Sampling $[G_{1:\hat{p}}|Y, \hat{p}]$

Require: Set of responses $V_y = (y_i, \ldots, y_n)$ and lagged attributes $V_z = (z_1, \ldots, z_{n\hat{p}})$
Initialize $G^{(1)}_{1:\hat{p}} = \emptyset$
for $y_i \in V_y$ **do**
    for $z_j \in V_z$ **do**
        Compute $\phi_a = P(Y|G^{(1)}_{y_i,\emptyset|1:\hat{p}})$ and $\phi_b = P(Y|G^{(1)}_{y_i,z_j|1:\hat{p}})$
        if $\phi_b > \phi_a$ **then** $G^{(1)}_{y_i,z_j|1:\hat{p}} = 1$ **else** $G^{(1)}_{y_i,z_j|1:\hat{p}} = 0$

for $h = 2$ to Total iterations **do**
    for $y_i \in V_y$, set $G^{(*)}_{y_i|1:\hat{p}} = G^{(h-1)}_{y_i|1:\hat{p}}$ **do**
        Randomly draw $z_k \sim V_z$
        Add/remove link from z_k to y_i: $G^{(*)}_{y_i,z_k|1:\hat{p}} = 1 - G^{(h-1)}_{y_i,z_k|1:\hat{p}}$
        Compute $\phi = \exp\,[\,\log P(Y|G^{(*)}_{y_i|1:\hat{p}}) - \log P(Y|G^{(h-1)}_{y_i|1:\hat{p}})\,]$. Draw $u \sim \mathcal{U}(0,1)$.
        if $u < \min\{1, \phi\}$ **then** $G^{(h)}_{y_i|1:\hat{p}} = G^{(*)}_{y_i|1:\hat{p}}$ **else** $G^{(h)}_{y_i|1:\hat{p}} = G^{(h-1)}_{y_i|1:\hat{p}}$

Algorithm 2 Sampling $[G_0|Y, \hat{G}_{1:\hat{p}}, \hat{p}]$

Require: Set of attributes $V_y = (y_i, \ldots, y_n)$ and estimated lag network $\hat{G}_{1:\hat{p}}$
Initialize $G^{(1)}_0 = \emptyset$ and $G^{(1)}_{0:\hat{p}} = [G^{(1)}_0, \hat{G}_{1:\hat{p}}]$
for $y_i \in V_y$ **do**
    Set $V_{y_i} = V_y \backslash \{y_i\}$ and $\{z_\pi : \hat{G}_{y_i,z_\pi|1:\hat{p}} = 1\}$
    for $y_j \in V_{y_i}$ **do**
        Set $\pi_i = (y_j \cup z_\pi)$. Compute $\phi_a = P(Y|G^{(1)}_{y_i,z_\pi|0:\hat{p}})$ and $\phi_b = P(Y|G^{(1)}_{y_i,\pi_i|0:\hat{p}})$
        if $\phi_b > \phi_a$ **then** $G^{(1)}_{y_i,\pi_i|0:\hat{p}} = 1$ **else** $G^{(1)}_{y_i,z_\pi|0:\hat{p}} = 1$

for $h = 2$ to Total iterations **do**
    for $y_i \in V_y$, set $G^{(*)}_{y_i|0:\hat{p}} = G^{(h-1)}_{y_i|0:\hat{p}}$ **do**
        Randomly draw $y_k \sim V_{y_i}$
        Add/remove link from y_k to y_i: $G^{(*)}_{y_i,y_k|0:\hat{p}} = 1 - G^{(h-1)}_{y_i,y_k|0:\hat{p}}$
        Compute $\phi = \exp\,[\,\log P(Y|G^{(*)}_{i|0:\hat{p}}) - \log P(Y|G^{(h-1)}_{i|0:\hat{p}})\,]$. Draw $u \sim \mathcal{U}(0,1)$.
        if $u < \min\{1, \phi\}$ **then** $G^{(h)}_{y_i|0:\hat{p}} = G^{(*)}_{y_i|0:\hat{p}}$ **else** $G^{(h)}_{y_i|0:\hat{p}} = G^{(h-1)}_{y_i|0:\hat{p}}$

Appendix B. Network Statistics

Average Degree

Average degree is simply the average number of edges per node in the graph. It can be computed numerically as: Average Degree = Total Edges/Total Nodes.

Network Density

Let A be an n-node graph without self-loop. We characterize (through numerical summaries) the time-varying nature of interconnections by monitoring the network density: Network Density = Total Edges/$n(n-1)$.

Clustering Coefficient

Network clustering index is a measure of the tendency for nodes in a network form clusters or triangles. We apply the global clustering index of Barrat and Weigt (2000) which corresponds to the social network concept of transitivity and can be captured numerically as:

$$CC = \frac{3 \times (\text{number of triangles})}{(\text{number of open triads})} \tag{B.1}$$

where open triads are defined as a connected sub-graph consisting of three nodes and two edges. The index takes values between 0 and 1. It can be viewed as the probability of two neighbors of a node link to each other.

Average Path Length

The average path length is the average number of steps along the shortest paths for all possible pairs of network nodes. The average path length for a network with n-nodes is

$$APL = \frac{1}{n(n-1)} \sum_{i \neq j} d_{i,j} \tag{B.2}$$

where $d_{i,j}$ is the shortest path between the nodes i and j.

Node Centrality

Node centrality in networks addresses the questions of how important a node/variable is in the network. Commonly discussed centrality measures include in-degree (number of in-bounds links), out-degree (number of out-bound links), authority, and hub scores. Let A^w be an n-node weighted graph without self-loop.

1. The authority score of node-i is a weighted sum of the power/hub score of the vertices with directed links towards node-i. They can be obtained via absolute value of the eigenvectors associated with the largest eigenvalue of $(A^w A^{w'})$. An authority node has a large in-degree.
2. The hub score of node-j is the weighted sum of the power/authority score of vertices with a directed link from node-j. They can be obtained via absolute value of the eigenvectors associated with the largest eigenvalue of $(A^{w'} A^w)$. A hub node usually has a large out-degree.

From a financial viewpoint, nodes with high authority scores/in-degree are highly influenced by others, while high hub scores/out-degree nodes are the influencers.